

Synthetic Aperture Communication: Principles and Application to Massive IoT Satellite Uplink

Lucas Giroto, Marcus Henninger, and Silvio Mandelli

Nokia Bell Labs Stuttgart, 70469 Stuttgart, Germany

E-mail: {firstname.lastname}@nokia-bell-labs.com

Abstract—While synthetic aperture radar is widely adopted to provide high-resolution imaging at long distances using small arrays, the concept of coherent synthetic aperture communication (SAC) has not yet been explored. This article introduces the principles of SAC for direct satellite-to-device uplink, showcasing precise direction-of-arrival estimation for user equipment (UE) devices, facilitating spatial signal separation, localization, and easing link budget constraints. Simulations for a low Earth orbit satellite at 600 km orbit and two UE devices performing orthogonal frequency-division multiplexing-based transmission with polar coding at 3.5 GHz demonstrate block error rates below 0.1 with transmission powers as low as -10 dBm, even under strong interference when UE devices are resolved but fall on each other’s strongest angular sidelobe. These results validate the ability of the proposed scheme to address mutual interference and stringent power limitations, paving the way for massive Internet of Things connectivity in non-terrestrial networks.

Index Terms—6G, direct satellite-to-device (DS2D), non-terrestrial networks (NTN), orthogonal frequency-division multiplexing (OFDM), synthetic aperture communication (SAC).

I. INTRODUCTION

Direct satellite-to-device (DS2D) communication has gained attention as a solution for reliable links between ground user equipment (UE) and satellite receivers [1]. These scenarios involve UEs with limited transmission power and satellite receivers with constrained beamforming. Addressing similar challenges, [2] described a narrowband (NB) Internet of Things (IoT) uplink (UL) scenario with a ground UE transmitting signals to a satellite receiver in the low Earth orbit (LEO). The analysis therein showed that, despite adopting a transmit power of 23 dBm and covering a narrow bandwidth of 180 kHz at 2 GHz, robust channel coding yielding data rates as low as 4.6 kbps is needed to counter severe path loss and limited UE antenna and array gains. When interference from terrestrial base stations, UE devices, or other satellite UE devices arises, countermeasures such as radio resource management or multiplexing are typically used [3], trading off data rate for robustness without adding further capabilities to the DS2D UL.

To address these challenges, this article proposes a novel coherent synthetic aperture communication (SAC) system concept. As in Wi-Fi and future sixth generation (6G) standards, orthogonal frequency-division multiplexing (OFDM) is used as reference waveform. Then, synthetic aperture radar (SAR)-based processing is leveraged to make the experienced time-varying Doppler shift due to satellite movement constant,

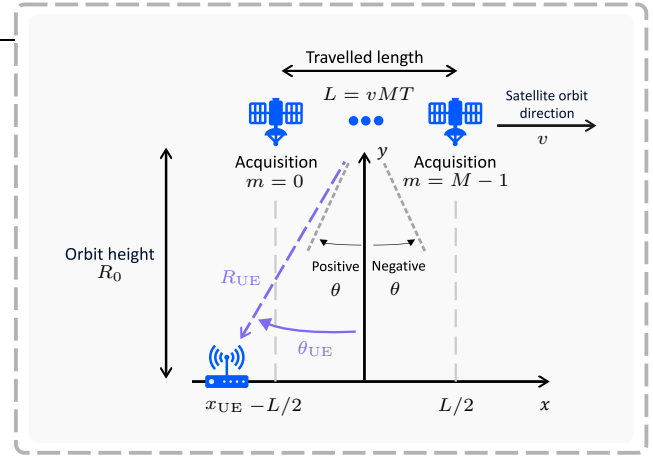


Fig. 1. Satellite UL with LoS between a ground UE at $x = x_{UE}$ and $y = 0$ and a satellite at orbit height R_0 moving with orbital velocity v from $x = -L/2$ to $x = L/2$ at $y = R_0$. From the middle point of the satellite’s trajectory to the UE, a range R_{UE} and an azimuth angle θ_{UE} are observed.

enabling coherent processing of consecutively acquired OFDM symbol copies. Thanks to the satellite displacement, this forms a synthetic aperture providing coherent processing gain and enabling fine direction-of-arrival (DoA) estimation. The latter facilitates estimating the direction of UE devices and separating their signals in the angular domain, therefore also handling interference. The proposed concept differs from SAC approaches in underwater acoustic communication (UWAC), which rely on incoherent diversity combining [4]. These approaches require long acquisition intervals for diversity, lack DoA estimation, and do not address multi-user interference.

The proposed SAC system concept can significantly advance DS2D UL capabilities, extending beyond currently envisioned use cases such as text messaging. It supports robust, low-data-rate communication and precise positioning in an integrated sensing and communication (ISAC) context, with DoA estimation enabling fine cross-range resolutions. In addition, it supports massive IoT applications in the non-terrestrial networks context, facilitating UL communication between low-power or battery-limited UE devices and receivers with well-defined trajectories, such as satellites.

II. SYSTEM MODEL

Let a satellite at an orbit height R_0 moving with orbital velocity v along the x axis as in Fig. 1 act as a receiver in

an UL scenario with bandwidth B and carrier frequency f_c , where the transmitter is a static UE. Furthermore, OFDM-based communication is assumed, with a discrete-frequency domain frame $\mathbf{S} \in \mathbb{C}^{N \times M}$ containing M OFDM symbols with N subcarriers each being transmitted by the UE. By performing inverse discrete Fourier transforms (IDFTs) along the columns of \mathbf{S} , the discrete-time domain OFDM frame $\mathbf{s} \in \mathbb{C}^{N \times M}$ is generated. Next, a cyclic prefix (CP) of length N_{CP} is prepended to each of the M OFDM symbols in the columns of \mathbf{s} . The resulting discrete-time domain frame then undergoes parallel-to-serial (P/S) conversion, digital-to-analog (D/A) conversion and further analog conditioning, yielding the complex baseband UE transmit signal $s(t) \in \mathbb{C}$ with transmit power P_{Tx} . Additional relevant parameters of the OFDM signal are its subcarrier spacing, symbol duration with CP, and frame duration. The former is given by $\Delta f = B/N$. As for the latter two, they are defined as $T = T_0 + T_{\text{CP}}$, where $T_0 = 1/\Delta f = N/B$ is the OFDM symbol duration without CP and $T_{\text{CP}} = N_{\text{CP}}/B$ is the CP duration, and $T_{\text{frame}} = M T = M(N + N_{\text{CP}})/B$, respectively.

During the M acquisitions of OFDM symbols with duration T , the satellite travels a length $L = v M T$. It is henceforth assumed that the length L traveled by the satellite is between $x = -L/2$ to $x = L/2$ at the orbit height R_0 , and that the UE is located at $x = x_{\text{UE}}$ on the ground. The time-varying x coordinate of the satellite is therefore $x(t) = (-L/2) + vt$. Consequently, the range between the UE and the satellite is

$$R(t) = \sqrt{(x(t) - x_{\text{UE}})^2 + R_0^2}. \quad (1)$$

After $s(t)$ being transmitted by the UE with transmit antenna gain G_{Tx} , and propagating through a line-of-sight (LoS) path, the complex baseband representation of the satellite receive signal $r(t) \in \mathbb{C}$ captured by a receive antenna of gain G_{Rx} is

$$r(t) = \sqrt{G_{\text{Tx}} G_{\text{Rx}}} \alpha(t) s(t - \tau(t)) e^{j\phi(t)} + \eta(t). \quad (2)$$

In this equation, $\alpha(t)$ is the time-varying attenuation that is influenced by path loss, atmospheric gas absorption losses, and ionospheric or tropospheric scintillation losses [5]. Lastly, $\eta(t) \in \mathbb{C}$ is the additive white Gaussian noise (AWGN). In non-line-of-sight (NLoS) cases, building entry losses are also considered. Furthermore, $\tau(t)$ is the time-varying delay experienced by the UL signal expressed as $\tau(t) = R(t)/c_0$, where c_0 is the speed of light in vacuum. $\phi(t) = 2\pi f_c \tau(t) = 2\pi f_c R(t)/c_0$ denotes the carrier phase, which is time varying due to the satellite movement. Based on (2) and recalling that $x(t) = (-L/2) + vt$, it holds that

$$\phi(t) = 2\pi f_c \frac{\sqrt{(-\frac{L}{2} + vt - x_{\text{UE}})^2 + R_0^2}}{c_0}. \quad (3)$$

For simplicity, it is henceforth assumed that the satellite is flying right above the UE and that the traveled length L , and therefore also vt , is negligible compared to the satellite altitude R_0 , i.e., $L \ll R_0$. Since $L = v M T$, $L \ll R_0$ can be achieved with the transmission of a short number of OFDM symbols M for a given orbital velocity v and OFDM

symbol duration T . Consequently, a time-invariant attenuation α and a time-invariant range $R_{\text{UE}} = \sqrt{x_{\text{UE}}^2 + R_0^2}$ and delay $\tau = R_{\text{UE}}/c_0$ are experienced. With larger M and therefore larger apertures, however, range migration may happen and must be corrected [6]. The time-varying behavior of the carrier $\phi(t)$ is kept, but for $L \ll R_0$ and knowing that $c_0 = \lambda f_c$, where λ is the wavelength associated with the carrier frequency f_c , it can be simplified as

$$\phi(t) = 2\pi \frac{\left[\left(-\frac{L}{2} + vt - x_{\text{UE}} \right)^2 / (2R_0) \right] + R_0}{\lambda}. \quad (4)$$

Consequently, (2) becomes

$$r(t) = \sqrt{G_{\text{Tx}} G_{\text{Rx}}} \alpha s \left(t - \frac{R_{\text{UE}}}{c_0} \right) \cdot e^{j2\pi \frac{\left[\left(-\frac{L}{2} + vt - x_{\text{UE}} \right)^2 / (2R_0) \right] + R_0}{\lambda}} + \eta(t). \quad (5)$$

Based on the expression of $\phi(t)$ in (4), the experienced time-varying Doppler shift $f_{\text{D}}(t)$ by $r(t)$ can be calculated as

$$f_{\text{D,UE}}(t) = \frac{1}{2\pi} \frac{d}{dt} \phi(t) = -\frac{\left(v \frac{L}{2} + x_{\text{UE}} \right)}{R_0 \lambda} + \frac{v^2 t}{R_0 \lambda}. \quad (6)$$

III. COHERENT SYNTHETIC APERTURE COMBINING

In the considered DS2D UL scenario, each UE transmits M copies of the same OFDM symbol. While this results in a data rate reduction by a factor of M , it allows exploiting the time-varying Doppler shift experienced due to the satellite movement to synthesize a virtual aperture for the satellite receiver. Although not required, ideal synchronization is assumed, and the processing in the SAC system is described as follows.

A. Azimuth compression

After analog conditioning, analog-to-digital (A/D) conversion, and serial-to-parallel (S/P) conversion, the CP is removed from all M OFDM symbols. The resulting receive OFDM frame in the discrete-time domain is denoted by $\mathbf{r} \in \mathbb{C}^{N \times M}$. The n th sample, $n \in \{0, 1, \dots, N-1\}$, of the m th OFDM symbol, $m \in \{0, 1, \dots, M-1\}$, which is located in row n and column m of \mathbf{r} , is given by

$$r_{n,m} = r(t)|_{t=mT+T_{\text{CP}}+n/B}. \quad (7)$$

Next, to eventually make the experienced time-varying Doppler shift $f_{\text{D,UE}}(t)$ constant, azimuth compression is performed along the OFDM symbols in \mathbf{r} . Still assuming pure LoS between UE and satellite, this is done by multiplying every sample $r_{n,m}$ by $h_{\text{az},n,m} = e^{-j\phi_{\text{az},n,m}}$, in which

$$\phi_{\text{az},n,m} = 2\pi \frac{\left\{ \left[-\frac{L}{2} + v \left(mT + T_{\text{CP}} + \frac{n}{B} \right) \right]^2 / (2R_0) \right\} + R_0}{\lambda} \quad (8)$$

is the phase response according to (4) for an UE at $x_{\text{UE}} = 0$ m on the ground [6] evaluated at the m th OFDM symbol, which starts at $t = mT + T_{\text{CP}}$. This operation results in the matrix

$\mathbf{r}_{\text{az}} \in \mathbb{C}^{N \times M}$, whose element $r_{\text{az},n,m} = r_{n,m} h_{\text{az},n,m}$ at its n th row and m th column is equal to

$$r_{\text{az},n,m} = \sqrt{G_{\text{Tx}} G_{\text{Rx}}} \alpha s \left(\left(mT + T_{\text{CP}} + \frac{n}{B} \right) - \frac{R_{\text{UE}}}{c_0} \right) \\ \cdot e^{j \frac{2\pi}{R_0 \lambda} \left[\frac{x_{\text{UE}}^2 + L x_{\text{UE}}}{2} - v x_{\text{UE}} \left(mT + T_{\text{CP}} + \frac{n}{B} \right) \right]} \\ + \eta_{n,m} e^{-j \phi_{\text{az},n,m}}. \quad (9)$$

In this equation, $\eta_{n,m} \in \mathbb{C}$ is a Gaussian random variable with mean $\mathbb{E}\{\eta_{n,m}\} = 0$ and variance $\mathbb{E}\{|\eta_{n,m}|^2\} = \sigma_\eta^2$ that represents the effect of the AWGN $\eta(t)$ in the n th row and m th column of \mathbf{r}_{az} . The resulting noise $\eta_{n,m} e^{-j \phi_{\text{az},n,m}}$ in this equation is henceforth denoted as $\eta_{\text{az},n,m} \in \mathbb{C}$, and it has the same mean and variance as $\eta_{n,m}$, i.e., $\mathbb{E}\{\eta_{\text{az},n,m}\} = 0$ and $\mathbb{E}\{|\eta_{\text{az},n,m}|^2\} = \sigma_\eta^2$. Furthermore, as all M transmit OFDM symbols are equal as assumed at the beginning of this section, (9) can be simplified and rearranged as

$$r_{\text{az},n,m} = \sqrt{G_{\text{Tx}} G_{\text{Rx}}} \alpha s \left(\left(T_{\text{CP}} + \frac{n}{B} \right) - \frac{R_{\text{UE}}}{c_0} \right) \\ \cdot e^{j \frac{2\pi}{R_0 \lambda} \left(\frac{x_{\text{UE}}^2 + L x_{\text{UE}}}{2} \right)} e^{j 2\pi \left(\frac{-v x_{\text{UE}}}{R_0 \lambda} \right) \left(mT + T_{\text{CP}} + \frac{n}{B} \right)} \\ + \eta_{\text{az},n,m}. \quad (10)$$

An analysis of this equation reveals that a Doppler shift $f_{\text{D,UE}}$ is experienced, which is expressed as

$$f_{\text{D,UE}} = -\frac{v x_{\text{UE}}}{R_0 \lambda}. \quad (11)$$

As previously mentioned, the ultimately experienced Doppler shift $f_{\text{D,UE}}$ results from the time-varying one $f_{\text{D,UE}}(t)$, which is made constant by the performed azimuth compression.

B. Doppler shift estimation

By performing discrete Fourier transforms (DFTs) along the columns of \mathbf{r}_{az} , a matrix $\mathbf{y}_{\text{az}} \in \mathbb{C}^{N \times M}$ is obtained, whose element at its n th row and l th column, $l \in \{-M/2, -M/2 + 1, \dots, M/2 - 1\}$, is given by

$$y_{\text{az},n,l} = \frac{1}{\sqrt{M}} \sqrt{G_{\text{Tx}} G_{\text{Rx}}} \alpha s \left(\left(T_{\text{CP}} + \frac{n}{B} \right) - \frac{R_{\text{UE}}}{c_0} \right) \\ \cdot e^{j \frac{2\pi}{R_0 \lambda} \left(\frac{x_{\text{UE}}^2 + L x_{\text{UE}}}{2} \right)} e^{j 2\pi \left(\frac{-v x_{\text{UE}}}{R_0 \lambda} \right) \left(T_{\text{CP}} + \frac{n}{B} \right)} \\ \cdot \sum_{m=0}^{M-1} e^{-j \frac{2\pi}{M} \left(l + \frac{v x_{\text{UE}} T M}{R_0 \lambda} \right)} + \eta'_{\text{az},n,l}. \quad (12)$$

In this equation, $\eta'_{\text{az},n,l}$ is the DFT of $\eta_{\text{az},n,m}$, which has the same mean $\mathbb{E}\{\eta'_{\text{az},n,m}\} = 0$ and variance $\mathbb{E}\{|\eta'_{\text{az},n,m}|^2\} = \sigma_\eta^2$ since the DFT was normalized.

Next, the Euclidean norm of the columns of \mathbf{y}_{az} is taken to produce the vector $\mathbf{y}_{\text{az, norm}} \in \mathbb{C}^{1 \times M}$. Based on (12), a maximum occurs at the \hat{l}_{UE} th column of $\mathbf{y}_{\text{az, norm}}$, $\hat{l}_{\text{UE}} \in \{-M/2, -M/2 + 1, \dots, M/2 - 1\}$, such that

$$\hat{l}_{\text{UE}} = -\frac{v x_{\text{UE}} T M}{R_0 \lambda}. \quad (13)$$

The Doppler shift resolution Δf_{D} for DFT-based estimation in an OFDM-based system is given by

$$\Delta f_{\text{D}} = \frac{1}{T_{\text{frame}}} = \frac{1}{M T}. \quad (14)$$

Knowing that Δf_{D} is equal to the Doppler shift bin width, the sample estimate \hat{l}_{UE} calculated according to (13) is associated with a Doppler shift estimate $\hat{f}_{\text{D,UE}} = \hat{l}_{\text{UE}} \Delta f_{\text{D}}$, which for high signal-to-noise ratio (SNR) is approximately equal to f_{D} .

C. Azimuth estimation

To convert the Doppler shift estimate $\hat{f}_{\text{D,UE}}$ into an azimuth estimate, the angle θ_{UE} in radians of the UE w.r.t. to the point in the center of the satellite trajectory during the transmission of the M OFDM symbols, i.e., $x = 0$ m at the orbit height R_0 , can be calculated based on Fig. 1 as

$$\theta_{\text{UE}} = \arcsin \left(\frac{x_{\text{UE}}}{\sqrt{x_{\text{UE}}^2 + R_0^2}} \right) \stackrel{|x_{\text{UE}}| \ll R_0}{=} \frac{x_{\text{UE}}}{R_0}. \quad (15)$$

Combining (11) and (15) allows expressing the azimuth estimate $\hat{\theta}_{\text{UE}}$ for the UE as

$$\hat{\theta}_{\text{UE}} = -\frac{\hat{f}_{\text{D,UE}} \lambda}{v}. \quad (16)$$

The expression in (16) shows that, by exploiting the experienced Doppler shift by the movement of the satellite receiver, a virtual array is synthesized, and angular estimation is enabled.

D. Azimuth resolution and ambiguity

Based on (14) and (16), the azimuth resolution associated with the virtual array is given by

$$\Delta \theta = \frac{\lambda}{v M T} = \frac{\lambda}{L}. \quad (17)$$

This equation allows interpreting the traveled length L by the satellite as the synthetic aperture length [6].

A further relevant parameter is the maximum unambiguous azimuth. It is derived from the maximum unambiguous Doppler shift for DFT-based estimation in an OFDM-based systems and expressed as

$$\theta_{\text{max,ua}} = \pm \frac{\lambda}{2 v T} = \pm \frac{M}{2} \Delta \theta. \quad (18)$$

It is worth highlighting that residual carrier frequency offset (CFO) may cause angular estimates to be biased or folded around the unambiguous azimuth range. Even so, UE devices with angular separation of at least $\Delta \theta$ can still be resolved.

E. Further communication processing

The processing on the matrix \mathbf{r}_{az} to extract the modulation symbols transmitted by the UE is described as follows. First, a Doppler shift correction is performed by multiplying \mathbf{r}_{az} by the steering vector $\mathbf{b}(\theta) \in \mathbb{C}^{M \times 1}$ evaluated for the obtained azimuth estimate $\hat{\theta}_{\text{UE}}$. Considering that the distance $d = v T$ traveled by the satellite between the transmission of consecutive OFDM symbols is equal to the antenna element spacing in the synthesized array

with synthetic aperture and that $\sin(\theta) \approx \theta$ for small θ , the element at the m th row of the receive steering vector is defined as $b_m(\theta) = (1/\sqrt{M}) e^{j\frac{2\pi}{\lambda} m v T \theta}$. Performing receive beamsteering of \mathbf{r}_{az} for the azimuth estimate $\hat{\theta}_{UE}$ yields $\mathbf{r}_{\hat{\theta}_{UE}} \in \mathbb{C}^{N \times 1} | \mathbf{r}_{\hat{\theta}} = \mathbf{r}_{az} \mathbf{b}(\hat{\theta}_{UE})$. Next, $\mathbf{r}_{\hat{\theta}_{UE}}$ undergoes Doppler shift correction by multiplying each n th element with $e^{-j2\pi \hat{f}_{D,UE} \frac{n}{B}}$. Based on (11) and assuming an ideal Doppler shift estimate $\hat{f}_{D,UE} = f_{D,UE}$, this complex exponential is equal to $e^{j\frac{2\pi}{R_0 \lambda} v x_{UE} \frac{n}{B}}$. This operation results in the vector $\mathbf{r}_{\hat{\theta}_{UE,D}} \in \mathbb{C}^{N \times 1}$, which after undergoing DFT results in $\mathbf{R}_{\hat{\theta}_{UE,D}} \in \mathbb{C}^{N \times 1}$. The k th element of $\mathbf{R}_{\hat{\theta}_{UE,D}}$ is given by

$$R_{\hat{\theta}_{UE,D},k} = \sqrt{G_{p,az}} \left[\sqrt{G_{Tx} G_{Rx}} \alpha S_k e^{-j\frac{2\pi k}{N} \left(\frac{R_{UE} B}{c_0} \right)} \cdot e^{j\frac{2\pi}{R_0 \lambda} \left(\frac{x_{UE}^2 + L x_{UE}}{2} \right)} e^{j2\pi \left(\frac{-v x_{UE}}{R_0 \lambda} \right) T_{CP}} \right] + \eta_{\hat{\theta}_{UE,D},k}, \quad (19)$$

where S_k is the transmit modulation symbol at the k th subcarrier of one of the M repeated OFDM symbols and $\eta_{\hat{\theta}_{UE,D},k}$ is the noise component which has the same mean $\mathbb{E}\{\eta_{\hat{\theta}_{UE,D},k}\} = 0$ and variance $\mathbb{E}\{|\eta_{\hat{\theta}_{UE,D},k}|^2\} = \sigma_\eta^2$ as the one in \mathbf{r}_{az} since beamsteering and DFT were normalized.

Assuming ideal channel state information (CSI) is available, zero forcing (ZF) equalization can be performed on $\mathbf{R}_{\hat{\theta}_{UE,D}}$ to yield $\mathbf{R} \in \mathbb{C}^{N \times 1} | \mathbf{R} = \mathbf{R}_{\hat{\theta}_{UE,D}} \odot \mathbf{G}$, where \odot is the Hadamard product and $\mathbf{G} \in \mathbb{C}^{N \times 1}$ is the ZF equalizer. For a pure LoS channel, the k th element of \mathbf{R} is given by

$$R_k = S_k + \eta'_{\hat{\theta}_{UE,D},k}, \quad (20)$$

where $\eta'_{\hat{\theta}_{UE,D},k}$ is the modified noise by the ZF equalizer, which, however, has unchanged mean $\mathbb{E}\{\eta'_{\hat{\theta}_{UE,D},k}\} = 0$ and variance $\mathbb{E}\{|\eta'_{\hat{\theta}_{UE,D},k}|^2\} = \sigma_\eta^2$. The noise variance is given by $\sigma_\eta^2 = N P_\eta$, where P_η is the AWGN power given by $P_\eta = k_B \Delta f T_{therm} \text{NF}$. In this equation, k_B is the Boltzmann constant, T_{therm} is the standard room temperature in Kelvin, and NF is the overall receiver noise figure in linear scale. Recalling that $B = N \Delta f$ and assuming uniform power allocation among the N subcarriers, the SNR associated with the estimate of the transmit modulation symbol S_k with (20) is

$$\text{SNR} = \frac{P_{Tx} G_{Tx} G_{Rx} G_{p,az} \alpha^2}{k_B B T_{therm} \text{NF}}. \quad (21)$$

IV. NUMERICAL ANALYSIS

In this section, the proposed coherent SAC system concept is verified via simulations. The satellite receiver is assumed to be in the LEO with orbit height $R_0 = 600$ km and orbital velocity $v = 7.82$ km/s. The channel model from [5] for a pure LoS case at $f_c = 3.5$ GHz is considered, with losses including a path loss of 158.89 dB, atmospheric absorption losses of 0.12 dB, and scintillation losses of 4.39 dB between UE transmitters at $y = 0$ m and the satellite receiver orbiting at $y = 600$ km, with negligible deviations during the satellite displacement along the x axis for the considered scenario. Combined, these yield a total propagation loss of 163.40 dB.

TABLE I
SYNTHETIC APERTURE COMMUNICATION SYSTEM PARAMETER REQUIREMENTS FOR SUB-KILOMETER CROSS-RANGE RESOLUTION

Δf	M	$G_{p,az}$	\mathcal{R}_b
15 kHz	≥ 93	≥ 19.68 dB	≤ 45.21 kbit/s ($B = 4.50$ MHz) ≤ 488.23 kbit/s ($B = 48.60$ MHz)
30 kHz	≥ 185	≥ 22.67 dB	≤ 20.00 kbit/s ($B = 3.96$ MHz) ≤ 496.40 kbit/s ($B = 98.28$ MHz)
60 kHz	≥ 369	≥ 25.67 dB	≤ 20.06 kbit/s ($B = 7.92$ MHz) ≤ 246.14 kbit/s ($B = 97.20$ MHz)

Next, it is assumed that each UE was equipped with a $\lambda/2$ -spaced uniform rectangular array (URA) with fixed array aperture of 8.56×8.56 cm², a gain of $G_{Tx} = 11.72$ dBi, and a half-power beamwidth (HPBW) of 50.6° [7]. For the satellite receiver, the gain of $G_{Rx} = 30$ dBi and the HPBW of 4.41° from Table 6.1.1.1-1 of the 3GPP TS 38.821 [8], as well as a noise figure NF = 4 dB [9] are assumed.

To further alleviate transmit power requirements of the SAC system in addition to the azimuth processing gain $G_{p,az}$ and ensure tolerable communication error rates, a Fifth Generation New Radio (5G NR) polar code with rate $\mathcal{R}_c = 2/3$ is henceforth adopted. In addition, 25% out of the total of N subcarriers are used as pilots in a regularly-spaced comb. After coherent synthetic aperture combining, these pilots are extracted and used for channel estimation. The obtained channel frequency response is then interpolated to cover all N subcarriers and enable subsequent equalization.

A. Synthetic aperture communication system parameters

For sub-kilometer cross-range resolution, a synthetic aperture length $L > 51.39$ m is required based on (17). For subcarrier spacings in Frequency Range 1 (FR1) numerologies $\mu = 0$ to $\mu = 2$ of 5G NR, this results in the requirements in Table I. For the performed simulations, standard-compliant normal CP durations were considered [10]. The numbers in Table I show that such fine resolution is associated with azimuth processing gains that significantly alleviate the link budget. This comes, however, at the cost of reduction of the net data rate \mathcal{R}_b by a factor of M compared to the case where no synthetic aperture is synthesized and different OFDM symbols are transmitted. Note that, although code spreading can achieve a similar trade-off between SNR improvement and data rate, it lacks the DoA estimation and angular resolution and user multiplexing capabilities inherent to the introduced SAC system concept.

B. Communication performance in multi-user scenario

Next, a scenario with 2 UE devices, labeled as UE #1 and UE #2, performing UL transmission with full time and frequency overlap is assumed. All previously adopted parameters are kept except for subcarrier spacing, bandwidth, and number of acquired OFDM symbol copies, which are set to $\Delta f = 15$ kHz, $B = 4.5$ MHz, and $M = 93$, respectively. Consequently, a synthetic aperture length $L = 51.88$ m is obtained, which is associated with an azimuth resolution of $\Delta\theta = (94.60 \cdot 10^{-3})^\circ$ and a maximum unambiguous azimuth of $\theta_{\max,ua} = \pm 4.40^\circ$. In addition, these values correspond to a

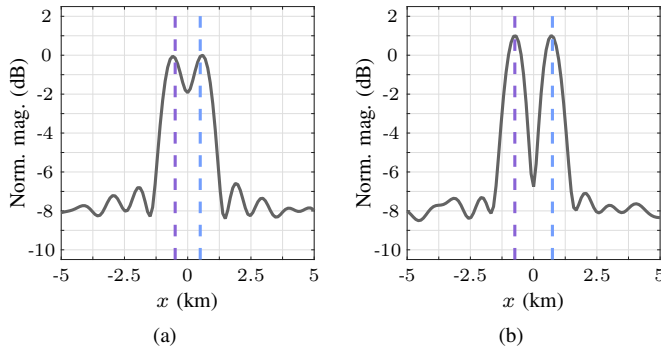


Fig. 2. Azimuth profile as a function of the x coordinate (—). For (a), two perfectly resolved UE devices are considered, $x_{UE,1} = -495.33$ m (—) and $x_{UE,2} = 495.33$ m (—). In (b), two resolved UE devices, $x_{UE,1} = -742.99$ m (—) and $x_{UE,2} = 742.99$ m (—), are considered. All magnitudes are normalized w.r.t. to the highest peak in (a).

cross range resolution of $R_0 \Delta\theta = 990.65$ m and a maximum unambiguous cross range of $R_0 \theta_{\max,ua} = \pm 46.07$ km.

Fig. 2 shows the result of the procedure to obtain the azimuth estimates $\hat{\theta}_{UE}$ and consequently x coordinate estimates of UE devices described in Sections III-A to III-B for a transmit power $P_{Tx} = -10$ dBm and two scenarios. These are, namely, $x_{UE,1} = -495.33$ m for UE #1 and $x_{UE,2} = 495.33$ m for UE #2 in Fig. 2(a), and $x_{UE,1} = -742.99$ m for UE #1 and $x_{UE,2} = 742.99$ m for UE #2 in Fig. 2(b). In the first, the UE devices are separated by 990.65 m, an integer multiple of the cross-range resolution, which allows full separability of their signals. In the second scenario, however, the cross-range difference between UE devices is 1.49 km, which is equal to $1.5 \cdot R_0 \theta_{\max,ua}$. This distance is not an integer multiple of the resolution and leads to the maximum azimuth sidelobe level of around -13.26 dB w.r.t. the main peak from one UE at the position of the other one, which is observed in the form of higher normalized magnitude at the UE cross ranges. Consequently, maximum mutual interference between resolved UE devices in the angular domain is experienced during the beamsteering described in Section III-E.

The results in Fig. 2 showed that resolving transmitting UE devices is possible with $P_{Tx} = -10$ dBm for the considered system parameters, which is possible since the energy of all M OFDM symbol copies is compressed into the azimuth bin due to azimuth compression and DFT processing, leading to a similar effect to SNR processing gain in radar systems, though not coherent. To evaluate the effect of the transmit power on the overall communication performance, Fig. 3 shows the achieved block error rate (BLER) as a function of P_{Tx} for the same scenarios as for Fig. 2. The achieved results show that $\text{BLER} \leq 0.1$ can be achieved with around $P_{Tx} \geq -10.33$ dBm for both UE devices in the first scenario due to ideal UE separation in the angular domain. As for the second scenario, the aforementioned interference due to azimuth sidelobes results in a slightly higher transmit power requirement of $P_{Tx} \geq -10.12$ dBm to achieve $\text{BLER} \leq 0.1$. Both scenarios present superior performance compared to the case without SAC by around 20 dB, which is due to the azimuth processing gain $G_{p,az} = 19.68$ dB traded off against

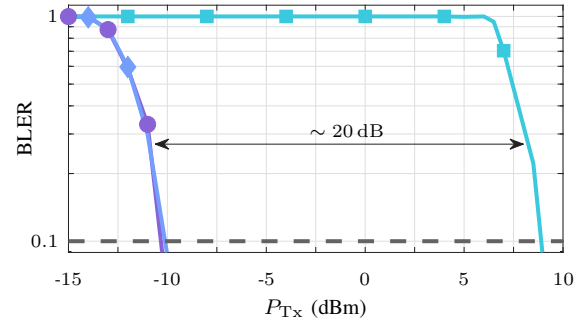


Fig. 3. Mean BLER for both UE devices as a function of the transmit power P_{Tx} for the scenario with $x_{UE,1} = -495.33$ m and $x_{UE,2} = 495.33$ m (—) and the scenario with $x_{UE,1} = -742.99$ m and $x_{UE,2} = 742.99$ m (—). For comparison, BLER curves for a single-UE scenario with both UE and satellite receiver at $x = 0$ m and without SAC (—) and a maximum tolerable BLER of 0.1 is highlighted (—) are also shown.

a data rate reduction by a factor of $M = 93$.

V. CONCLUSION

This article introduced a novel coherent SAC system concept for the DS2D UL. It involves a UE transmitting copies of a signal that are processed at a satellite receiver to form a synthetic aperture. This allows the receiver to estimate the UE direction, besides performing beamsteering and coherent combining. In addition to alleviating link budget requirements and enabling DoA estimation of multiple UE devices, the proposed SAC system concept effectively manages interference via spatial multiplexing, making it well-suited for massive IoT applications. Simulation results for a LEO satellite with an orbit height of 600 km and two UE devices at 3.5 GHz demonstrated that $\text{BLER} \leq 0.1$ is achieved for resolved UE devices in the angular domain for transmission powers of around -10 dBm or higher.

REFERENCES

- [1] T. S. Rappaport, T. E. Humphreys, and S. Nie, "Spectrum opportunities for the wireless future: from direct-to-device satellite applications to 6G cellular," *npj Wireless Technol.*, vol. 1, no. 1, p. 8, Dec. 2025.
- [2] M.-G. Kim and H.-S. Jo, "Performance analysis of NB-IoT uplink in low earth orbit non-terrestrial networks," *Sensors*, vol. 22, no. 18, Sept. 2022.
- [3] K. Ntontin et al., "A vision, survey, and roadmap toward space communications in the 6G and beyond era," *Proc. IEEE*, vol. 113, no. 9, pp. 987–1023, Sept. 2025.
- [4] C. He, R. Xi, H. Wang, L. Jing, W. Shi, and Q. Zhang, "Single carrier with frequency domain equalization for synthetic aperture underwater acoustic communications," *Sensors*, vol. 17, no. 7, Jul. 2017.
- [5] 3rd Generation Partnership Project (3GPP), "Study on New Radio (NR) to support non-terrestrial networks," TR 38.811, Jun. 2019, V15.1.0.
- [6] A. Moreira, P. Prats-Iraola, M. Younis, G. Krieger, I. Hajnsek, and K. P. Papathanassiou, "A tutorial on synthetic aperture radar," *IEEE Geosci. Remote Sens. Mag.*, vol. 1, no. 1, pp. 6–43, Mar. 2013.
- [7] Z. Cui, P. Zhang, and S. Pollin, "6G wireless communications in 7–24 GHz band: Opportunities, techniques, and challenges," in *2025 IEEE International Symposium on Dynamic Spectrum Access Networks (DySPAN)*, May 2025, pp. 1–8.
- [8] 3rd Generation Partnership Project (3GPP), "Solutions for NR to support non-terrestrial networks (NTN)," TR 38.821, Mar. 2023, V16.2.0.
- [9] H. Shahid et al., "Emerging advancements in 6G NTN radio access technologies: An overview," in *2024 Joint Eur. Conf. Netw. Commun. 6G Summit*, Jun. 2024, pp. 593–598.
- [10] 3rd Generation Partnership Project (3GPP), "Physical channels and modulation," TS 38.211, Jul. 2023, V17.5.0.